



# Changes of air pollutants and simulation of a heavy pollution process during COVID-19 in Shenyang

Yunfeng Ma · Huijie Zhao · Xiangnan Wei

Received: 24 April 2022 / Accepted: 11 August 2022 / Published online: 3 September 2022  
© The Author(s), under exclusive licence to Springer Nature Switzerland AG 2022

**Abstract** During COVID-19, Shenyang implemented strict household isolation measures, resulting in a sharp reduction in anthropogenic emission sources, providing an opportunity to explore the impact of human activities on air pollution. The period from January to April of 2020 was divided into normal period, blockade period and resumption period. Combined with meteorological and pollutant data, mathematical statistics and spatial analysis methods were used to compare with the same period of 2015–2019. The results showed that  $PM_{2.5}$ ,  $PM_{10}$ ,  $NO_2$  and  $O_3$  increased by 32.6%, 13.2%, 4.65% and 22.7% in the normal period, among which the western area changed significantly. During the blockade period, the concentration of pollutants decreased by 35.79%, 35.87%, 32.45% and -4.84%, of which the central area changed significantly. During the resumption period, the concentration of pollutants increased by 21.8%, 8.7%, 5.7% and -6.3%, and the area with the largest change was located in the western. During the blockade period, a heavy pollution occurred with  $PM_{2.5}$  as the main pollutant. The WRF-Chem model and the HYSPLIT model were used to reproduce the pollution occurrence process. The result showed that winds circulated as zonal winds during the pollution process at high altitudes. These winds were controlled by straight westerly and weak northwesterly

airflows in front of the high pressure, and the ground was located behind the warm low pressure. Weather conditions were relatively stable. Thus, high temperatures (average  $> 10$  °C), high humidity (40%-60%) and slow wind (2 m/s) conditions prevailed for a long time in the Shenyang area. The unfavorable meteorological conditions lead to the occurrence of pollution. The backward trajectory showed that the potential source areas were concentrated in the urban agglomeration around Shenyang, and sporadic contributions came from North Korea.

**Keywords** COVID-19 · Pollution · WRF-Chem · HYSPLIT

## Introduction

The sudden COVID-19 outbreak that occurred at the end of December 2019 represents a great threat to human safety and has attracted widespread attention around the world. In order to control the epidemic and reduce the spread of the virus to the greatest extent possible, various regions have implemented a series of strict control measures, which include blocking traffic roads, limiting non-essential activities of the population, as well as closing factories and schools, among others (Hu et al., 2021; Tian et al., 2021). The implementation of control measures has reduced atmospheric emissions from anthropogenic sources, providing an opportunity to investigate the

Y. Ma · H. Zhao (✉) · X. Wei  
Shenyang Aerospace University, Shenyang 110136, China  
e-mail: 1369881944@qq.com

extent to which air pollution is affected by human activities (Chen et al., 2021; Eyisi et al., 2021; Yan et al., 2021).

Changes in air pollution concentrations are affected by the combined effects of anthropogenic sources and meteorological conditions, and scholars have contributed many methods in the process of studying the characteristics of pollutants (Yin et al., 2021; Xue et al., 2021; Thangjai et al., 2021; Ma et al., 2019; Feistel & Hellmuth, 2021). Since the COVID-19 outbreak, domestic and foreign scholars have performed a significant amount of research to determine changes of air pollutants during the epidemic. Zhu et al. (2021) used the NAQPMS model and obtained scenario simulations to evaluate the emission reduction effect of the “2+26” program during the epidemic. According to their results, concentration of pollutants decreased during the epidemic (January 24<sup>th</sup> to March 31<sup>th</sup>), as compared to a pre-pandemic period (January 1<sup>st</sup> to 23<sup>th</sup>). In addition, meteorological conditions caused the PM<sub>2.5</sub> concentration in cities along the Yanshan and Taihang Mountains to increase by about 1% to 8%. Also, Zhou et al. (2020) used the continuous emission monitoring system (CEMS) to evaluate the relationship between air quality improvement and pollutant reduction during the epidemic. These researchers reported that during the epidemic, the average daily emissions of SO<sub>2</sub>, NO<sub>x</sub> and soot (PM) in key industries in Hubei Province decreased by 41.9%, 34.7% and 47.6%, respectively. Wu et al. (2020) studied the impact of strong control measures for various pollution sources on the atmospheric environment during the pneumonia epidemic. The results showed that during the epidemic period, the air quality index (AQI) decreased by 43% and 50%, respectively, as compared with the same period in 2018–2019. In addition, concentrations of NO<sub>2</sub>, PM<sub>10</sub> and PM<sub>2.5</sub> decreased by 72%, 53% and 45%, respectively. Zhao et al. (2021) analyzed the evolution of air pollutants during two heavy haze pollution processes in Beijing during the COVID-19 period and found that home isolation measures significantly impacted diurnal variation of PM<sub>2.5</sub> and black carbon (BC) concentrations. Moreover, such measures displayed a higher impact on CO, NO<sub>2</sub> and SO<sub>2</sub>. However, diurnal O<sub>3</sub> variation was not significantly impacted. The primary pollutants in the two heavy haze pollution processes were

PM<sub>2.5</sub>. Cai et al. (2021) used the chemical transport model WRF-Chem and the ensemble square root filter assimilation system to simultaneously assimilate the initial field of pollutant concentration and the pollution source emission framework. Using the high-resolution condition of 1 km, these researchers determined that PM<sub>2.5</sub> aerosol and NO source emissions decreased by 4.4% and 30%, respectively, as compared to January. While most studies found significant improvements in air quality, others found that heavily polluted weather had not disappeared during the epidemic period. In some cities, the air quality was worse than before. This may be because the effect of reducing the discharge of primary pollutants was offset by adverse weather conditions and the enhancement of secondary pollution.

This finding showed that during the epidemic control period, the air quality in cities improved to different degrees. However, because air pollution is a complex mechanism, the changes in pollutants in different regions were not the same. In addition, in some regions, pollutants showed an increasing trend instead of a decreasing one (He et al., 2021). Shenyang represents one of the cities with the fastest work and production resumption in the country. In this city, insufficient atmospheric capacity and unfavorable meteorological conditions represent important challenges to prevent and control air pollution.

At present, the research on atmospheric conditions during COVID-19 had a large spatial scale, and there were few studies on the small scale. At the same time, research related to air pollution in Shenyang was limited by the single research data, and there was lack of research on the changes of pollutants (PM<sub>2.5</sub>, PM<sub>10</sub>, NO<sub>2</sub>, O<sub>3</sub>) during COVID-19. Compared with the existing studies, the study covered the whole epidemic period (from January to April, 2020). The research contents were as follows: ① Taking the past 5 years (2015–2019) as a reference, statistical methods were used to analyze the temporal and spatial distribution characteristics of air pollutants during the same period in 2020, and identify the characteristics of air pollution under emission reduction conditions; ② Based on the WRF-Chem and HYSPLIT model, the causes of a typical heavy pollution event in February 2020 were analyzed. This study provided the decision-making reference for better planning of urban construction and rational layout of industrial zones in Shenyang.

**Data and methods**

According to Order No. 1 and Order No. 9 issued by the Liaoning province (Fig. 1), the control measures for the suspension of work, production and school activities were implemented in the whole province on January 26<sup>th</sup>, 2020. Later, on March 22<sup>th</sup>, 2020, all work and production activities resumed. The present study selected January to April 2020 as the research period, taking January as the normal period, February and March as the blockade period, and April as the resumption period. Pollutant mass concentrations and meteorological conditions in Shenyang in these three periods were compared with those of the same periods during 2015 to 2019 (5a). The 11 monitoring stations (Table 1) were distributed in different areas of Shenyang city (Fig. 2), covering the city center, suburbs and rural areas.

**Data source**

Pollutants data used in the present research were obtained from the Shenyang Academy of Environmental Sciences Research Institute. The daily concentrations of PM<sub>2.5</sub>, PM<sub>10</sub> and NO<sub>2</sub> refer to average daily concentrations. In the case of O<sub>3</sub> concentration, data correspond to the maximum 8 h average concentration.

Daily meteorological data were acquired from China’s ground meteorological stations released by the China meteorological data website (<http://data.cma.cn>). These included air temperature, air pressure, relative humidity, wind speed and precipitation, among others.

**Table 1** Monitoring sites

Site	Longitude (E)	Latitude (N)	Category
Senlinlu	123°41'01"	41.56'02"	Northern sub-urbs
ShenliaoXilu	123°14'40"	41.00'05"	Western city
Hunnandonglu	123°30'18"	41.44'26"	Southern city
Xiaoheyuan	123°28'04"	41.47'12"	Central city
Lingdongjie	123°25'35"	41.50'48"	Central city
Xinxiujie	123°25'23"	41.41'56"	Southern city
Yunonglu	123°35'45"	41.54'31"	Northern sub-urbs
Taiyuanjie	123°24'06"	41.47'50"	Central city
Donglinglu	123°35'25"	41.50'28"	Eastern suburbs
Wenhualu	123°23'41"	41.45'55"	Central city
Jingshenjie	123°22'42"	41.55'22"	Northern sub-urbs

The input data of the air quality model WRF-Chem corresponded to the GDAS (Global Data Assimilation System) meteorological reanalysis data jointly released by the National Centers for Environmental Prediction (NCEP) and the National Centers for Atmospheric Research (NCAR). (<ftp://arlftp.arlhq.noaa.gov/pub/archives/gdas1>).

The input data of HYSPLIT (Hybrid Single Particle Lagrangian Integrated Trajectory Model) backward trajectory model were obtained from the Global Data Assimilation System (GDAS) reanalysis data provided by NCEP ( <ftp://arlftp.arlhq.noaa.gov/pub/archives/gdas1/>). Data were available 4 times a day, at 0:00, 6:00, 12:00 and 18:00 (UTC, Universal Time).

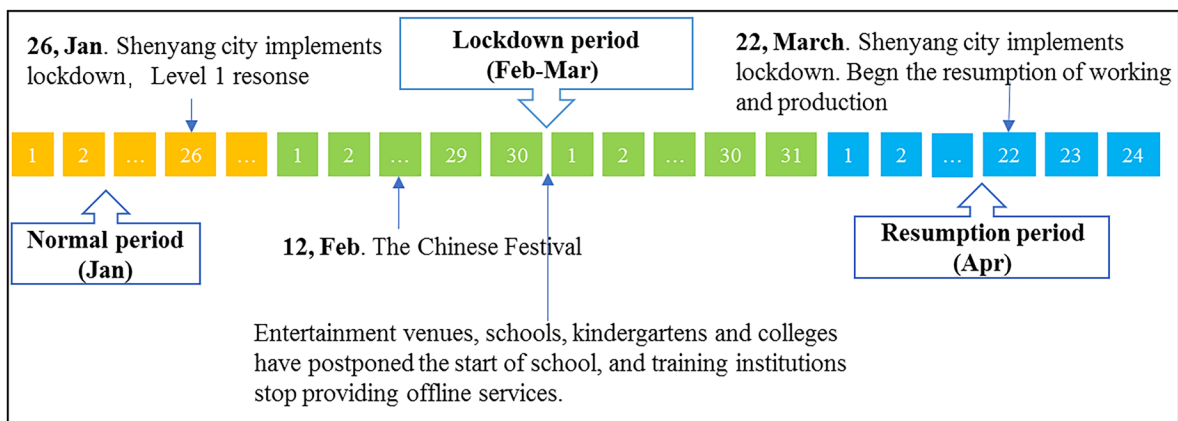


**Fig. 1** Timeline

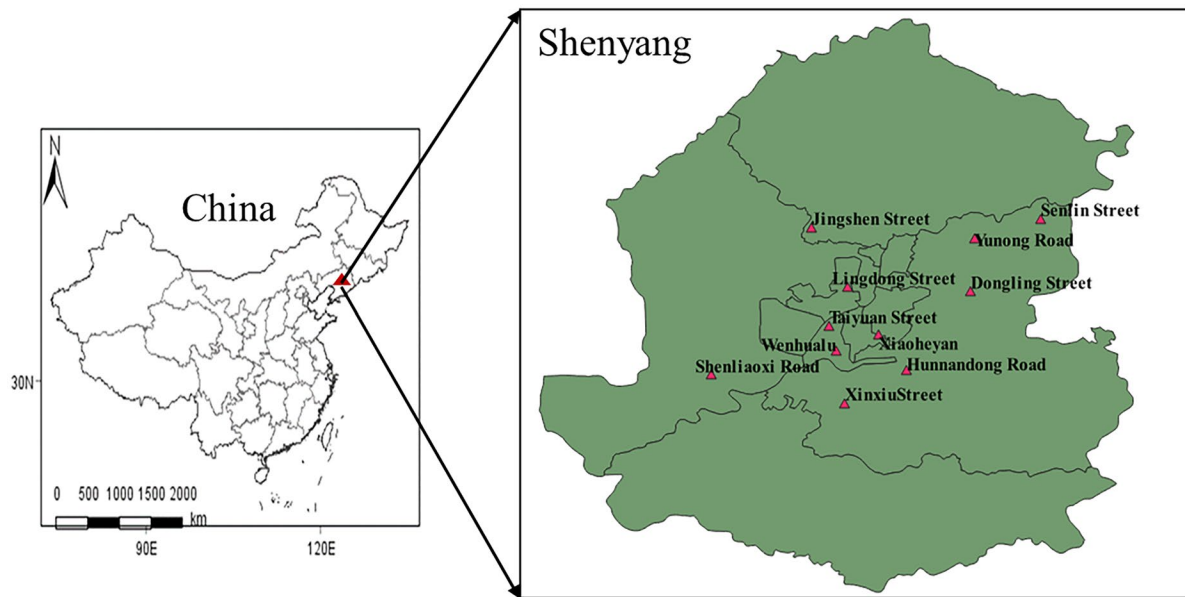


**Fig. 2** Study area

## Research method

### *WRF-Chem*

Shenyang city is located in the central region of Liaoning Province, and its geographic location is between 122°25′09″E–123°48′24″E and 41°11′51″N–43°02′13″N. We selected the Hunnan East Road in Shenyang city (41.44°N, 123.30°E) as the center point of the area. Also, we used Lambert projection coordinates and three-layer grid nesting. The setting of the entire grid nesting included Liaoning Province and the surrounding areas, and the innermost layer d03 with higher resolution was taken as the research object to improve the reliability of the results.

### *HYSPLIT*

PSCF (Potential Source Contribution Function) and CWT (Concentration Weighted Trajectory) analysis were performed using the HYSPLIT (Draxier & Hess, 1998) model. In addition, the Trajstat software developed by Wang et al. was used to determine the main sources and pollution trajectories, as well as to quantitatively analyze the contribution ratio of potential region to the pollution source in the target region. In order to simulate the source of the 48 h backward

trajectory, we selected a height of 100 m with respect to the ground as the base point. The Euclidean distance algorithm (Stohl, 1996; Dorling et al., 1992) was used to perform cluster analysis on all trajectories reaching the target point, and the total spatial variance (TSV) method was used to select the optimal number of clusters (Zhou et al., 2017). In order to reduce the uncertainty of PSCF and CWT results, the weight function  $W_{ij}$  was introduced according to the references (Hsu et al., 2003; Liu et al., 2021; Wang et al., 2022; Xia et al., 2021). Later, the final model results were analyzed according to the revised  $WPSCF = PSCF \times W_{ij}$  and  $WCWT = CWT \times W_{ij}$  data.

## Result and discussion

### Changes in pollutant concentrations

Figure 3 shows pollutants concentrations during the months of the pandemic corresponding to: (a) normal period; (b) lockdown period; and (c) resumption period in 2020, as well as average concentrations corresponding to the same months for the years of 2015–2019 (labeled as 5a). Data indicated that during the normal period in 2020, the concentrations of  $PM_{10}$ ,  $PM_{2.5}$ ,  $NO_2$ , and  $O_3$  were 13.2%, 32.6%, 4.65%,

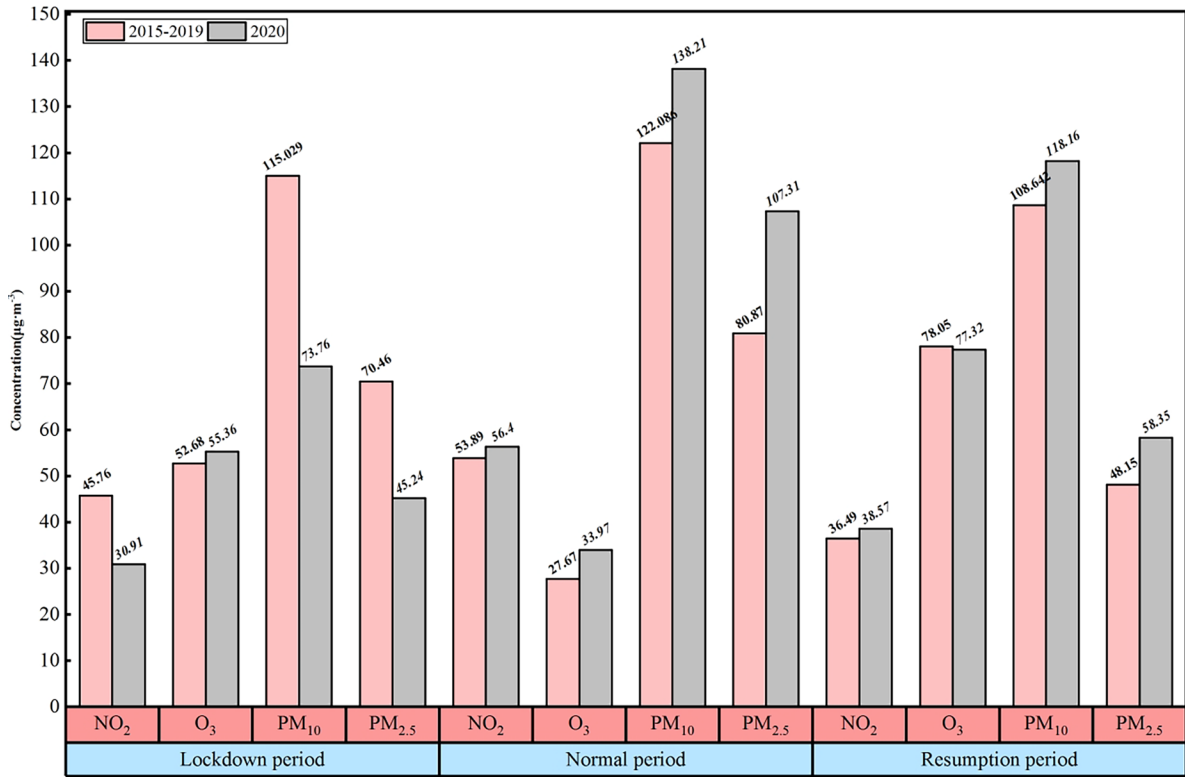


**Fig. 3** Comparison of pollutant concentrations in 2015–2019 and 2020

and 22.7% higher than those in 5a, respectively. The highest concentration changes corresponded to PM<sub>2.5</sub> and O<sub>3</sub>. The Spring Festival of China developed in late January 2020, during which a large number of fireworks and firecrackers were used. This time also corresponded with the heating period in Shenyang. For these reasons, pollutant concentrations increased.

During the blockade period, the concentrations of PM<sub>10</sub>, PM<sub>2.5</sub> and NO<sub>2</sub> were all lower than those observed in 5a. In this case, values decreased 35.87%, 35.79% and 32.45%, respectively. This occurred because of the large reduction of industry and traffic activities, which also reduced particulate matter and NOx emissions. However, O<sub>3</sub> showed a small increase of 4.84% during this period. Even under prevention and control conditions, the concentration of O<sub>3</sub> increased. This phenomenon was not only related to the decrease in PM<sub>2.5</sub> concentration, but also to the decrease in anthropogenic NOx emissions, which reduced the titration of O<sub>3</sub>. Since the absorption of HO<sub>2</sub> by the hydrolysis of high concentration of

NOx promotes the termination of the photochemical process, the concentration of O<sub>3</sub> decreased (Bao & Zhang, 2020). In addition, the response mechanism of O<sub>3</sub> to meteorological conditions in a certain concentration range is more complicated. The relationship between O<sub>3</sub> and meteorological factors slightly varied in different regions, but the effects of solar radiation, air temperature, temperature and humidity on O<sub>3</sub> were roughly the same (Toh et al., 2013). During the prevention and control period, the less rainy weather in Shenyang led to the increase in solar radiation, the increase in seasonal temperatures and the active photochemical reaction; thus, the concentration of O<sub>3</sub> increased.

During the resumption period, PM<sub>10</sub>, PM<sub>2.5</sub> and NO<sub>2</sub> concentrations were 8.7%, 21.8% and 5.7% higher, respectively, as compared with those observed in the corresponding period in 5a. In addition, O<sub>3</sub> concentration was 6.3% smaller as that in 5a. This probably occurred because in the late control stage, human activities resumed. Specifically, gradual return to

work and sudden increase in social activities occurred. As a consequence, traffic rate increased leading to an increase in pollutants concentrations. Moreover, the increase in  $\text{NO}_x$  concentration favored the titration of  $\text{O}_3$ , which caused a decrease in its concentration. Within a certain concentration range, the response mechanism of  $\text{O}_3$  to meteorological conditions is more complicated. During the prevention and control period, less rainy weather caused an increase in solar radiation. Also, the increase in seasonal temperatures favored atmospheric photochemical reactions and affected the structure of the boundary layer.

Based on the above analysis, it was found that  $\text{PM}_{2.5}$ ,  $\text{PM}_{10}$  and  $\text{NO}_2$  were more sensitive to the response to pollutant emission reduction during the epidemic period, and the pollutant  $\text{PM}_{2.5}$  was the most sensitive to the response to emission reduction. The correlation between  $\text{O}_3$  concentration and emission reduction was not obvious and had a certain hysteresis.

#### Spatial variation of pollutants

Figure 4 shows the concentration of pollutants in the Shenyang monitoring stations selected for the present research. Data indicated that concentrations of  $\text{PM}_{2.5}$ ,  $\text{PM}_{10}$ ,  $\text{NO}_2$  and  $\text{O}_3$  during the normal 2020 period were higher as compared with the 5a averages. Moreover, the largest differences were observed in western cities where  $\text{PM}_{2.5}$ ,  $\text{PM}_{10}$ ,  $\text{NO}_2$ , and  $\text{O}_3$  levels were  $49.79 \mu\text{g}\cdot\text{m}^{-3}$ ,  $54.24 \mu\text{g}\cdot\text{m}^{-3}$ ,  $12.27 \mu\text{g}\cdot\text{m}^{-3}$  and  $0.12 \mu\text{g}\cdot\text{m}^{-3}$  higher, respectively. In addition, during the blockade period, all pollutants except  $\text{O}_3$ , showed lower concentrations than those in the normal 2020 period and the corresponding 5a period. It was also observed that the highest differences were obtained in central cities, where  $\text{PM}_{2.5}$ ,  $\text{PM}_{10}$  and  $\text{NO}_2$  levels decreased by  $23.94 \mu\text{g}\cdot\text{m}^{-3}$ ,  $42.54 \mu\text{g}\cdot\text{m}^{-3}$  and  $19.65 \mu\text{g}\cdot\text{m}^{-3}$ , respectively. On the contrary,  $\text{O}_3$  concentration increased  $5.52 \mu\text{g}\cdot\text{m}^{-3}$ . During the resumption period in western cities,  $\text{PM}_{2.5}$ ,  $\text{PM}_{10}$  and  $\text{NO}_2$  concentrations were significantly higher as those observed in the corresponding 5a period. In this case, concentration differences were  $23.03 \mu\text{g}\cdot\text{m}^{-3}$ ,  $35.63 \mu\text{g}\cdot\text{m}^{-3}$  and  $10.59 \mu\text{g}\cdot\text{m}^{-3}$ , correspondingly. Also, it was observed that  $\text{O}_3$  concentration decreased  $13.22 \mu\text{g}\cdot\text{m}^{-3}$ .

During the epidemic control period, pollutants concentrations in each functional area improved to different

degrees. In addition, the concentration trends of each pollutant in different periods varied. During the implementation of control measures, different types of pollution control should be implemented according to the pollution characteristics of different control areas. In addition, the control of  $\text{PM}_{2.5}$  and  $\text{PM}_{10}$  pollution in western cities,  $\text{O}_3$  in urban suburbs, and  $\text{NO}_2$  in central cities should be strengthened.

#### Analysis of weather conditions

For analytical purposes, in the present research we selected  $\text{PM}_{2.5}$  as the primary pollutant in the Shenyang area. It has been reported that  $\text{NO}_2$  is a critical pollutant for a variety of chemical reactions that occur in the atmosphere. For example, this gas is a precursor in the formation of  $\text{O}_3$  and secondary aerosols. In Shenyang, traffic emissions represent the main source of  $\text{NO}_2$ , which are greatly affected by human activities. For these reasons, we also included  $\text{NO}_2$  as a representative pollutant.

Previous studies have shown that large-scale reductions in road transport and industrial emissions can significantly improve local air quality, and the complexity of the pollution source made it was more difficult to target (Angelevska et al., 2021). Meteorological conditions may improve air circulation and in consequence, the transport, retention and superposition of aerosol particles with those locally produced (Yao et al., 2017; Yu et al., 2015). Thus, air pollutants concentrations are directly and indirectly affected. Figure 5 displays the meteorological conditions observed from January to April 2020 and the average values of the same period in 5a. Data indicated that temperature, dew point temperature, air pressure and wind speed increased in 2020, as compared with 5a. On the whole, the fluctuation range of meteorological conditions was small.

By comparing pollutants concentrations over the same period, it was determined that although Shenyang implemented a series of control measures during the epidemic, the changes in pollutant concentrations were quite different. According to the air quality standard (GB3095-2012), the secondary standard concentration limits for  $\text{PM}_{2.5}$  and  $\text{O}_3$  are  $75 \mu\text{g}\cdot\text{m}^{-3}$  and  $80 \mu\text{g}\cdot\text{m}^{-3}$ , respectively. Figure 6a shows that the number of days that  $\text{PM}_{2.5}$  concentration exceeded the standard value ( $\rho \geq 75 \mu\text{g}\cdot\text{m}^{-3}$ ) were 21 and 9 in January and April of 2020, respectively, with average

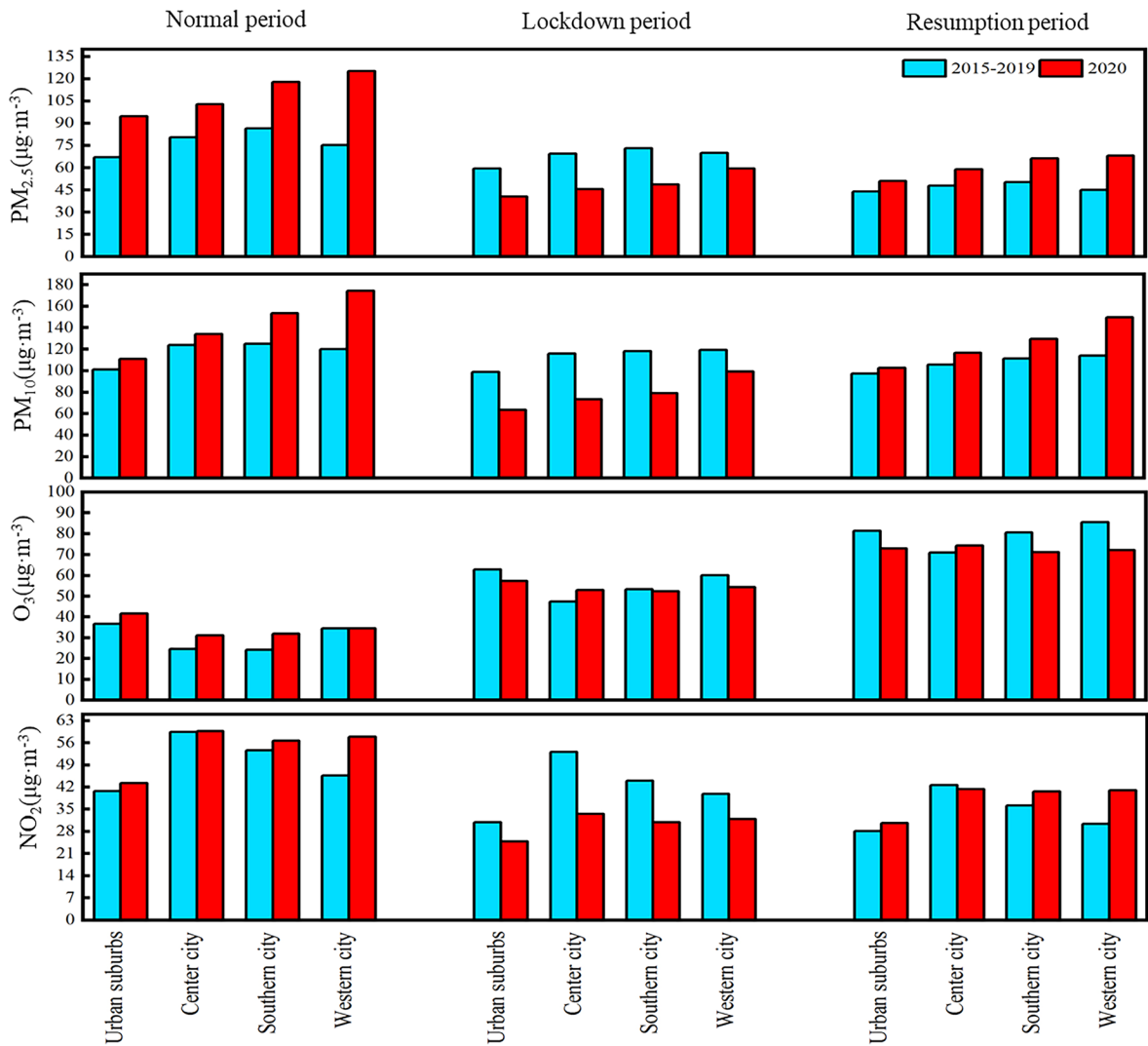


**Fig. 4** Comparison of pollutant concentrations in each functional area in 2015–2019 and 2020

concentrations of 107.23 µg·m<sup>-3</sup> and 58.35 µg·m<sup>-3</sup>, correspondingly. In addition, the occurrence frequency of polluted weather in January and April in 2020 was second only to the most polluted year in 2015. Data also indicated that PM<sub>2.5</sub> exceeded the standard level 6 d in February and 2 d in March, 2020, with average concentrations of 49.46 µg·m<sup>-3</sup> and 39.38 µg·m<sup>-3</sup>, correspondingly. Figure 6b displays the frequency of days NO<sub>2</sub> overpassed the standard value ( $\rho \geq 80 \mu\text{g}\cdot\text{m}^{-3}$ ). As data show, in 2016 and 2018 NO<sub>2</sub> concentrations did not exceed the standard value. Also, the number of days NO<sub>2</sub> concentrations surpassed the standard limit in 2015

was higher as compared to the other years. In January 2020, NO<sub>2</sub> concentration exceeded the standard limit for a total of 5 d, with an average concentration of 56.40 µg·m<sup>-3</sup>. In February and March, NO<sub>2</sub> concentrations decreased to 28.81 µg·m<sup>-3</sup> and 31.42 µg·m<sup>-3</sup>, respectively. Thus, in this period, standard limit was not exceeded. In April, the society resumed work and production, and the concentration of NO<sub>2</sub> increased. However, average concentration was 38.57 µg·m<sup>-3</sup> with no days exceeding the standard value.

In order to investigate the meteorological conditions occurring in Shenyang from January to April at 2020, we obtained the meteorological time series diagram

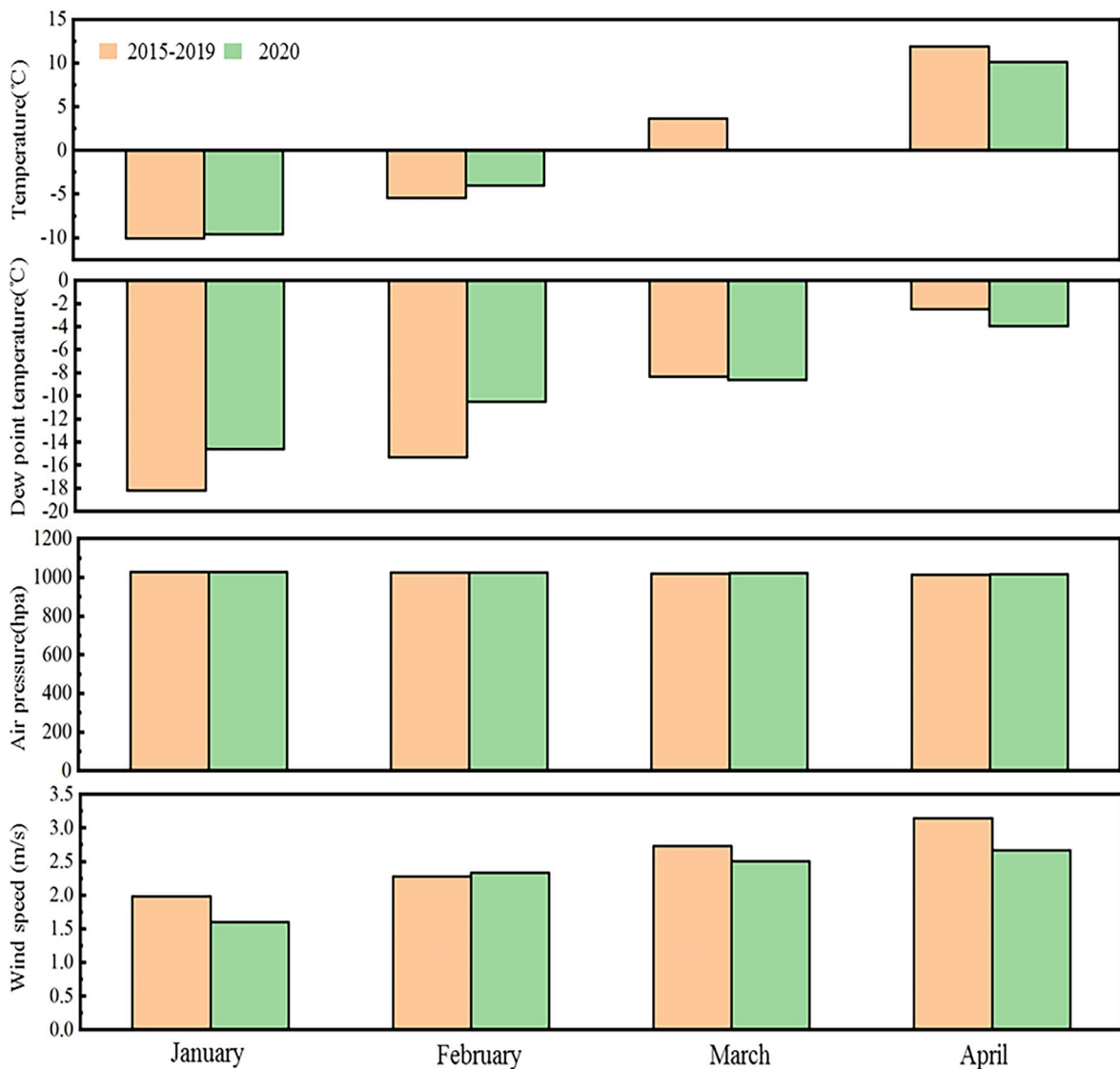


**Fig. 5** Comparison of meteorological elements between 2015–2019 and 2020

shown in Fig. 7. Results indicated that in 2020, the average temperature was  $-0.8674\text{ }^{\circ}\text{C}$ , the average wind speed was  $2.27\text{ m/s}$ , the air pressure was  $1023.03\text{ hpa}$ , and the average humidity was about  $57\%$ . The overall weather did not favor the removal and diffusion of pollutants. In February, different levels of polluted weather occurred in Shenyang, and a typical heavy pollution process was observed from February 8<sup>th</sup> to February 12<sup>th</sup>. During the haze event, the humidity in Shenyang was relatively high, and temperature significantly increased. Thus, a temperature inversion

layer easily formed. The temperature inversion layer reduced the atmospheric boundary layer, which hindered the vertical diffusion of pollutants (Hua et al., 2018; Wang et al., 2010; Wu et al., 2019). The pollution event was closely related to changes in air pressure, and surface air pressure reflects the intensity of cold air activity (Li & Xiang, 2018). The air pressure decreased, and the wind speed was relatively small. For this reason, pollutants were not removed.

Table 2 presents the correlation coefficient matrix of  $\text{PM}_{2.5}$  and  $\text{NO}_2$  concentrations and various meteorological

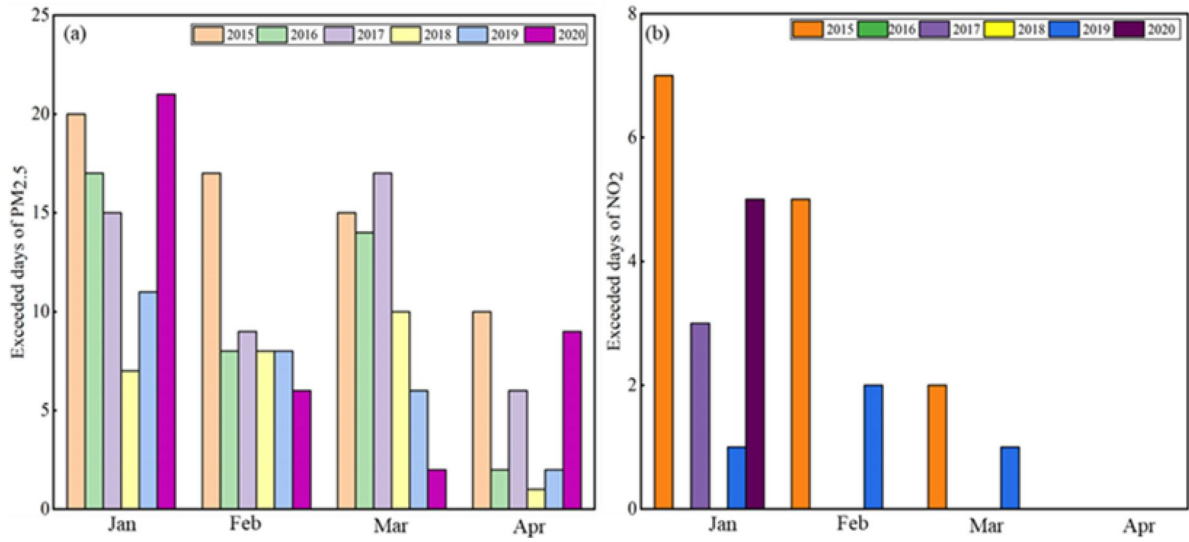


Fig. 6 Number of days standard pollutant concentration values were exceeded in 2020 and 2015–2019

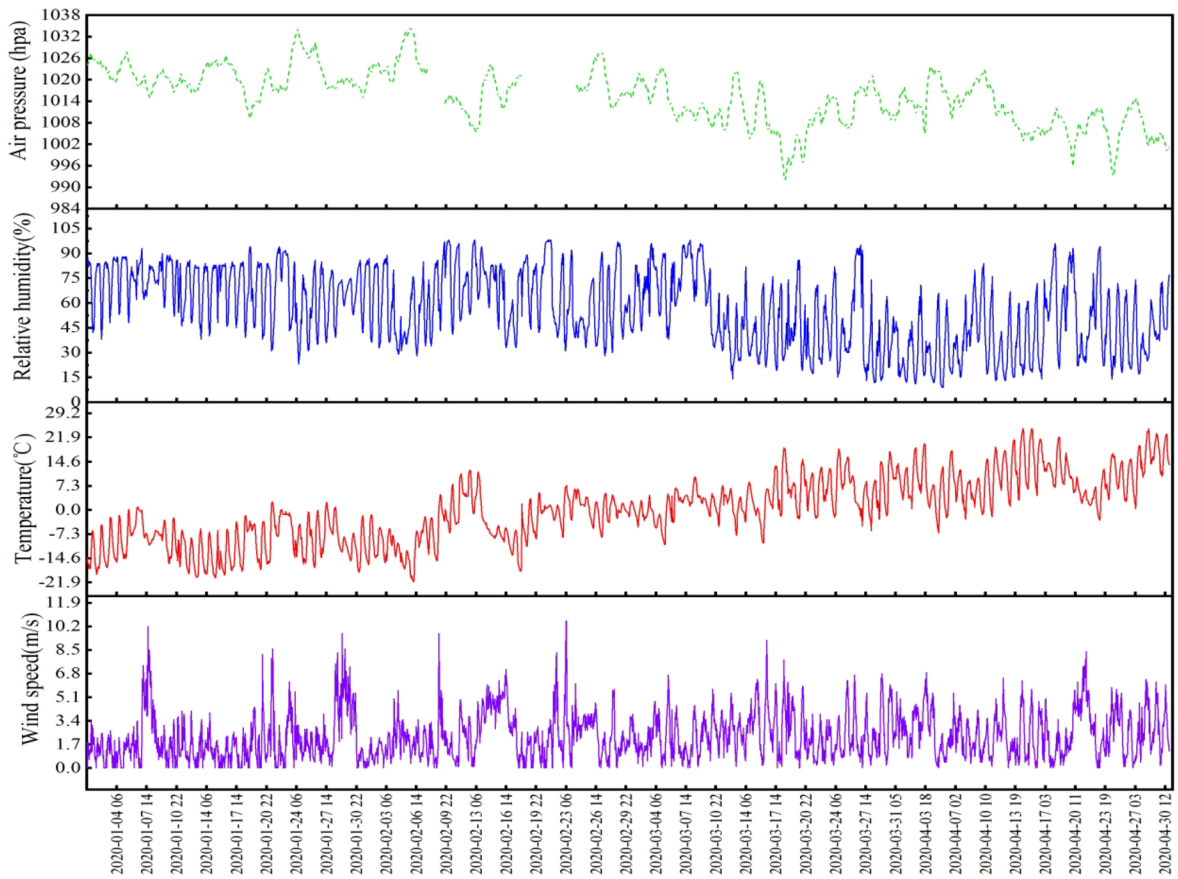


Fig. 7 Meteorological changes from January to April, 2020

**Table 2** Correlation between pollutant concentrations and meteorological factors

	PM <sub>2.5</sub>	NO <sub>2</sub>	Temperature	Relative humidity	Pressure	Wind speed
PM <sub>2.5</sub>	1	0.7432**	-0.2898**	0.3499**	0.2360**	-0.3093**
NO <sub>2</sub>		1	-0.2989**	0.3872**	0.1760**	-0.5614**
Air temperature			1	-0.5975**	-0.7348**	0.3140**
Relative humidity				1	0.2591**	-0.4144**
Pressure					1	-0.2297**
Wind speed						1

\*\*indicates a significant correlation at the 0.01 level (two-tailed)

factors from January to April of 2020. As results indicated, a significant correlation between each factor was observed, which indicated that meteorological factors indirectly affected the concentration of pollutants to a certain extent. However, the sensitivity of different pollutants to the influence of meteorological conditions is different. These results are consistent with the conclusions published in previous studies (Guo et al., 2015). Humidity and air pressure were positively correlated with PM<sub>2.5</sub> and NO<sub>2</sub> concentrations, while temperature and wind speed were negatively correlated with PM<sub>2.5</sub> and NO<sub>2</sub> concentrations. Among them, the correlation coefficient between relative humidity and PM<sub>2.5</sub> (0.3499) was relatively high. Also, the correlation coefficient between wind speed and NO<sub>2</sub> (-0.5614) was relatively high. These data proved that relative humidity and wind speed have significant effects on the removal and accumulation of PM<sub>2.5</sub> and NO<sub>2</sub>, respectively. Comparing the correlation coefficient between pollutants (PM<sub>2.5</sub>, NO<sub>2</sub>) and meteorology, it was found that the NO<sub>2</sub> concentration was more sensitive to the meteorological conditions such as humidity, temperature and wind speed during the study period. This is because NO<sub>2</sub> is a primary pollutant, and its transformation process is more dependent on meteorological conditions. The NO<sub>2</sub> concentration had a more significant response to human emission reduction and was more affected by meteorological conditions than the secondary pollutant PM<sub>2.5</sub>.

**Table 3** Correlation between air pollutants concentrations

	PM <sub>2.5</sub>	PM <sub>10</sub>	CO	O <sub>3</sub>	SO <sub>2</sub>	NO <sub>2</sub>
PM <sub>2.5</sub>	1	0.8716**	0.8040**	-0.0982	0.7918**	0.7432**
PM <sub>10</sub>		1	0.6862**	0.0610	0.6880**	0.6336**
CO			1	-0.2764**	0.8473**	0.8324**
O <sub>3</sub>				1	-0.2199*	-0.1870*
SO <sub>2</sub>					1	0.7710**
NO <sub>2</sub>						1

\* indicates a significant correlation at the 0.05 level (two-tailed); \*\*indicates a significant correlation at the 0.01 level (two-tailed)

Table 3 shows the results of the correlation analysis between different pollutants from January to April 2020. Data indicated that, except for O<sub>3</sub>, PM<sub>2.5</sub> displayed a significant correlation with each pollutant at the 0.01 level. The highest correlation coefficient (0.8716) was that between PM<sub>2.5</sub> and PM<sub>10</sub>. This is related to the fact that PM<sub>2.5</sub> is a component of PM<sub>10</sub>, both of which are particulate matter and have similar sources. With respect to NO<sub>2</sub>, the highest correlation occurred with CO. NO<sub>2</sub> is mainly originated from traffic sources, and CO from incomplete combustion. At present, combustion of petroleum fuel in transportation activities represents the main source of pollutants. It is important to note that insufficient combustion of petroleum produces CO. For this reason, NO<sub>2</sub> and CO display high correlation. Data also indicated that PM<sub>2.5</sub> and NO<sub>2</sub> were negatively correlated with O<sub>3</sub>. A potential explanation is that the extremely low socio-economic background greatly favored the reduction of NO<sub>x</sub> emissions. For this reason, titration effect of O<sub>3</sub> decreased and the increase in temperature promoted the generation of O<sub>3</sub>. Thus, the relationship between NO<sub>2</sub> and O<sub>3</sub> can be described as “One increases, the other decreases.”

In different concentration levels of PM<sub>2.5</sub> and NO<sub>2</sub>, the correlation between the concentration of PM<sub>2.5</sub> and relevant meteorological elements were analyzed. As shown in Table 4, during the heavy pollution period, there was a significant positive correlation

between PM<sub>2.5</sub> concentration and wind speed, which was inconsistent with the meteorological conditions of quiet wind in heavy pollution events. During the blockade period in 2020, the overall wind speed in Shenyang was relatively small, which was conducive to maintaining light pollution. However, the occurrence of heavy pollution events was related to the increase of local wind speed, which meant that the regional transport of pollutants was a potential impact of heavy pollution events. Mechanism, the increase of pollutants may mainly come from the transport contribution of adjacent regional pollution sources after discharge. Table 5 shows that in clean weather, NO<sub>2</sub> concentration was significantly negatively correlated with wind speed, and the correlation coefficient was -0.5443, indicating that wind speed had an obvious effect on NO<sub>2</sub> scavenging. Traffic emissions were one of the main sources of NO<sub>2</sub>. Therefore, in the future, Shenyang should vigorously develop public transportation to optimize the road structure, promote clean energy vehicles, build new transportation modes, and strengthen the control of motor vehicle emissions through traffic restrictions.

Analysis of heavy pollution cases during the epidemic

As shown in Fig. 8, during the epidemic blockade Shenyang experienced 4 different levels of pollution, including one severe pollution event ( $\rho(\text{PM}_{2.5}) \geq 150 \mu\text{g}\cdot\text{m}^{-3}$ ,  $\rho(\text{NO}_2) \geq 80 \mu\text{g}\cdot\text{m}^{-3}$ ). These processes were defined as P1, P2, P3, and P4, respectively. The primary pollutant in these events was PM<sub>2.5</sub>, and no NO<sub>2</sub> pollution was observed. The repetitive phenomenon of disappearance-increase-dissipation of pollutants occurred and P1 and P2 remained for a long period of time (>48 h). In addition, multiple peaks were observed in the intermediate process, indicating that P1 and P2 involved long-term accumulation of pollutants. The P1 and P2 periods

corresponded to strict control stage during the epidemic in Shenyang. Herein, anthropogenic and industrial sources of pollutants were significantly reduced. It was initially believed that the pollution process was related to unfavorable meteorological conditions. P3 and P4 pollution events had a remarkable common feature of short duration (<12 h), rapid outbreak and rapid dissipation. Shenyang proposed to gradually resume work and production activities on March 22<sup>th</sup>. Thus, P3 and P4 were related to the resumption of human activities. In addition, the peak and low concentration values of PM<sub>2.5</sub> and NO<sub>2</sub> in P1, P2, P3 and P4 were almost synchronous.

The above analysis showed that, compared with other pollution processes during the blockade period, the P1 process was a heavy pollution with PM<sub>2.5</sub> as the primary pollutant and had the longest duration. In order to gain an in-depth understanding of the mechanism of pollution in Shenyang, the P1 process was analyzed (Figs. 9, 10 and 11). Different from the pollution characteristics in the normal emission period of Shenyang, the peak time of P1 pollution was relatively short. During P1 pollution process, the real-time monitoring data (Fig. 9) showed AQI (mean) > 100,  $\rho(\text{PM}_{2.5}) > 86 \mu\text{g}\cdot\text{m}^{-3}$  and  $\rho(\text{NO}_2) > 39 \mu\text{g}\cdot\text{m}^{-3}$ . Figure 10 shows that the wind direction was predominantly from the southwest. On the 8<sup>th</sup> (Fig. 11a), the ground in Shenyang was controlled by the cold high-pressure center system in the north direction. In this region, sparse isobars, high pressure gradient and low wind speeds were observed. Since direction of surface winds was mainly northerly, diffusion of pollutants was not favored. On the 9<sup>th</sup>, the pollution level turned into heavy pollution, which remained for 18 h. During this period (Fig. 9), AQI (average) > 200,  $\rho(\text{PM}_{2.5}) > 78 \mu\text{g}\cdot\text{m}^{-3}$ ,  $\rho(\text{NO}_2) > 37 \mu\text{g}\cdot\text{m}^{-3}$ . According to Fig. 11b, a high-pressure divergent system occurred in the north part of the Liaoning Province, and a low-pressure composite system in the south area. In the Shenyang area, meteorological conditions deteriorated,

**Table 4** Correlation between different PM2.5 concentrations and meteorological elements

Concentration	Sample	Wind speed	Temperature	Humidity	Pressure
All Samples	2860	-0.3093**	-0.2898**	0.3499**	0.2360**
$\leq 75 \mu\text{g}\cdot\text{m}^{-3}$	2001	-0.3024**	-0.0902**	0.3872**	0.0192
$75 \mu\text{g}\cdot\text{m}^{-3} < \text{PM}_{2.5} \leq 150 \mu\text{g}\cdot\text{m}^{-3}$	650	-0.0803*	-0.1793**	0.1177**	0.0.1321**
$> 150 \mu\text{g}\cdot\text{m}^{-3}$	236	0.0626	-0.0189	-0.1501*	0.2476**

\* indicates a significant correlation at the 0.05 level (two-tailed); \*\*indicates a significant correlation at the 0.01 level (two-tailed)

**Table 5** Correlation between different NO<sub>2</sub> concentrations and meteorological elements

Concentration	Sample	Wind speed	Temperature	Humidity	Pressure
All Samples	2860	-0.5614**	-0.2988**	0.3871**	0.1760**
≤ 80 μg·m <sup>-3</sup>	2676	-0.5443**	-0.2791**	0.3891**	0.1641**
> 80 μg·m <sup>-3</sup>	211	-0.1522*	0.2002**	-0.1042	-0.1256*

\* indicates a significant correlation at the 0.05 level (two-tailed); \*\*indicates a significant correlation at the 0.01 level (two-tailed)

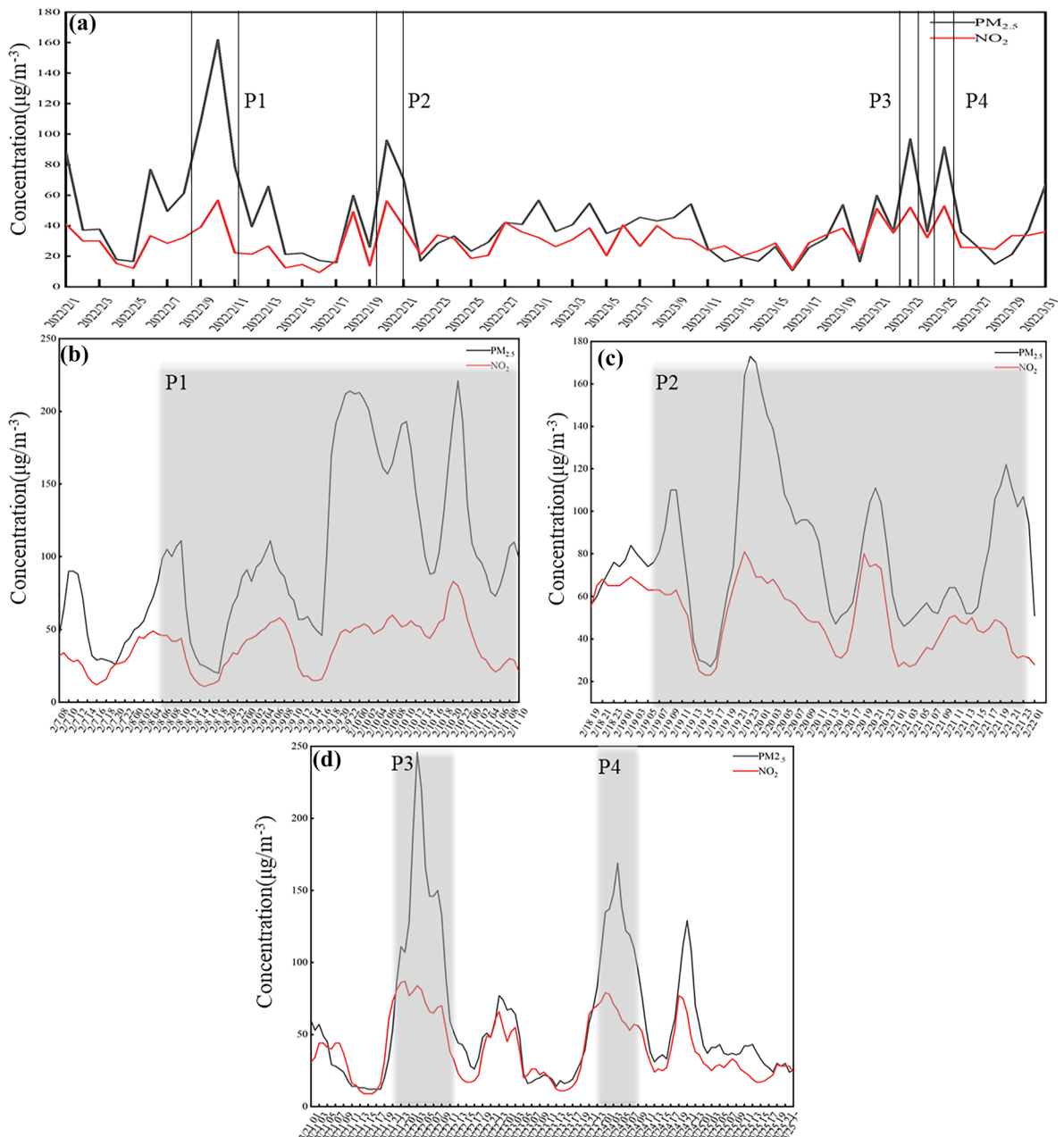


**Fig. 8** Statistical analysis of pollution incidents during the blockade period in 2020 (a) Concentration of pollutants of four pollution processes; (b) Concentration of pollutants in P1; (c) Concentration of pollutants in P2; (d) Concentration of pollutants in P3 and P4

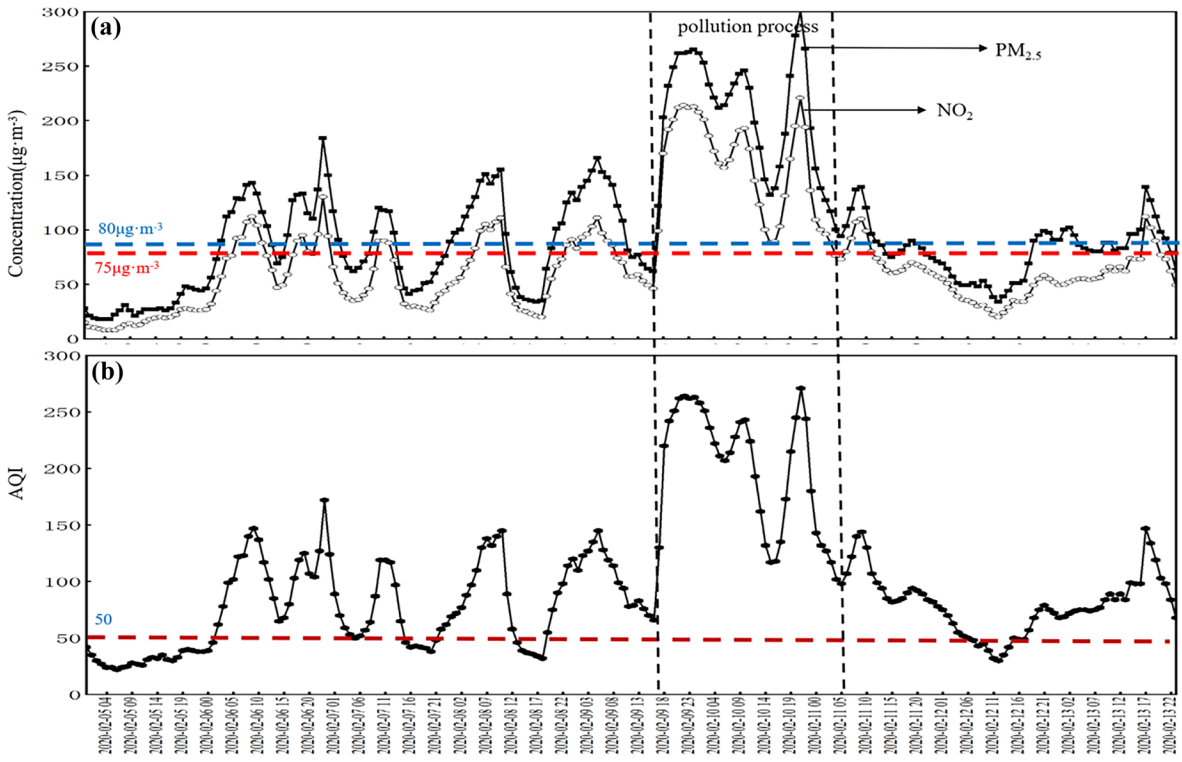


**Fig. 9** The changes of (a) pollutant concentrations and (b) AQI value in P1 pollution process

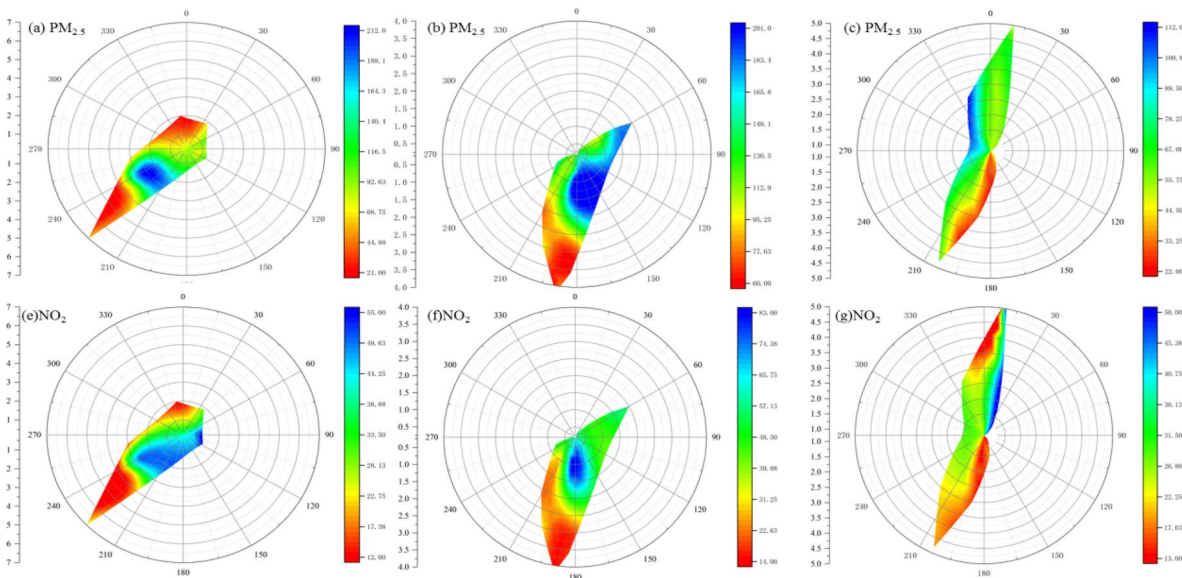


**Fig. 10** PM<sub>2.5</sub> and NO<sub>2</sub> pollution rose charts of P1 pollution process

and the air flow was prone to convection. Under the action of the southwest wind, the pollutants accumulated, and the pollution continued to increase. On the evening of the 9<sup>th</sup>,  $AQI > 240$ ,  $\rho(PM_{2.5}) > 200 \mu\text{g}\cdot\text{m}^{-3}$ ,  $\rho(\text{NO}_2) > 45 \mu\text{g}\cdot\text{m}^{-3}$ . Pollution continued on February 10<sup>th</sup>, where  $AQI$  (mean)  $> 208$ ,  $\rho(PM_{2.5}) > 157 \mu\text{g}\cdot\text{m}^{-3}$ ,  $\rho(\text{NO}_2) > 53 \mu\text{g}\cdot\text{m}^{-3}$ . The wind direction was mainly south-southwest, and the high-pressure center occurred in northeast Heilongjiang (Fig. 11c). The Shenyang area was affected by a weak high-pressure system, the isobars were sparse, and the surface wind speed was significantly reduced to below  $2 \text{ m}\cdot\text{s}^{-1}$ . Thus, the relatively stable weather system did not favor the diffusion and dilution of pollutants. On the night of February 10<sup>th</sup>, the heavy pollution turned into moderate pollution. At noon on February 11<sup>th</sup> (Fig. 9), the pollutants gradually

dissipated. Average  $AQI < 100$ ,  $\rho(PM_{2.5}) < 70 \mu\text{g}\cdot\text{m}^{-3}$  and  $\rho(\text{NO}_2) < 20 \mu\text{g}\cdot\text{m}^{-3}$ . The ground isobars were dense, high pressure gradient and wind speeds occurred, and the meteorological conditions improved. In this case, weather conditions favored the diffusion of pollutants (Fig. 11d). On February 12<sup>th</sup> (Fig. 9), the weather conditions improved with  $AQI < 55$ . During this period, southwesterly and northerly winds prevailed. The overall wind speed increased, atmospheric diffusion conditions improved and the pollution process ended. In the whole pollution process, the average concentration fluctuation of  $\text{NO}_2$  was lower than that of  $PM_{2.5}$ , indicating that the response sensitivity of secondary pollutant  $PM_{2.5}$  to artificial emission reduction was relatively weak compared with primary pollutant  $\text{NO}_2$ , with a certain lag.

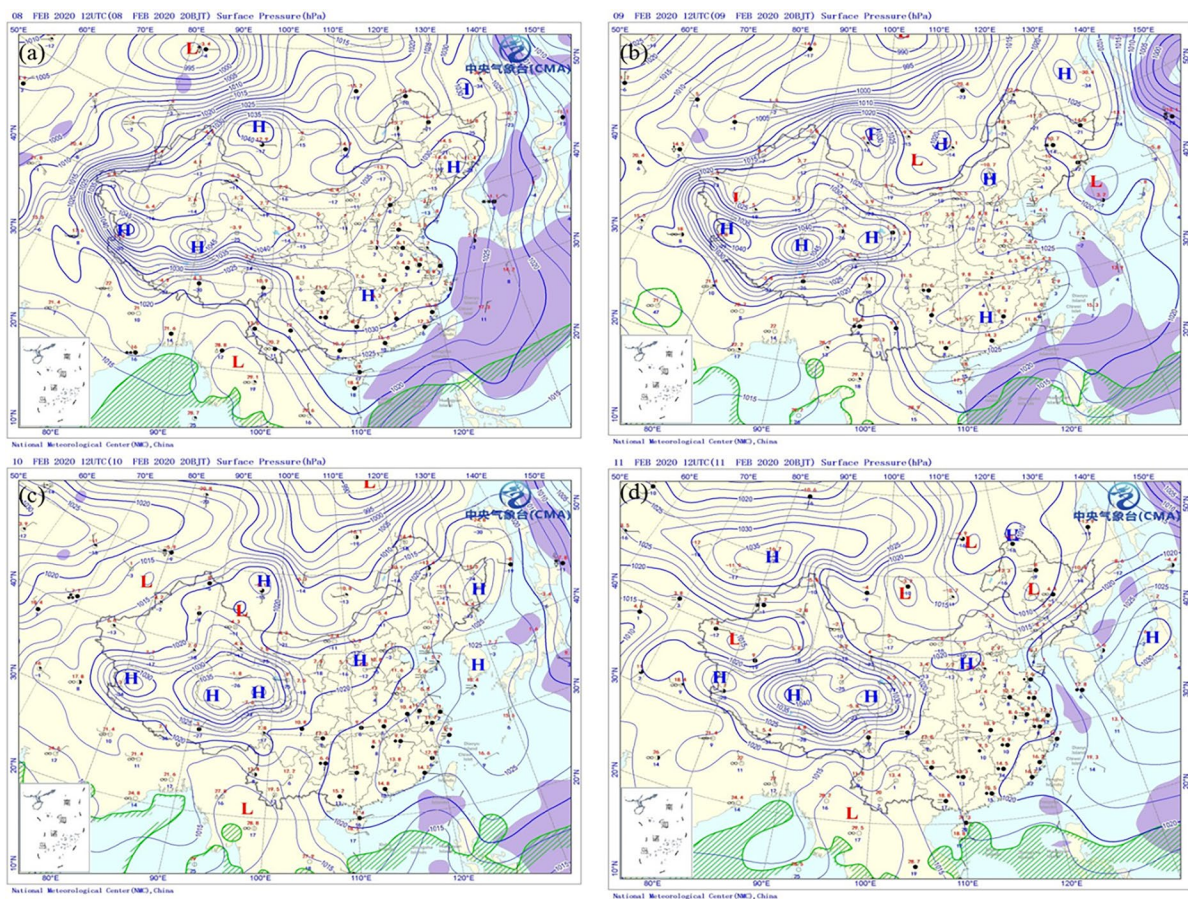


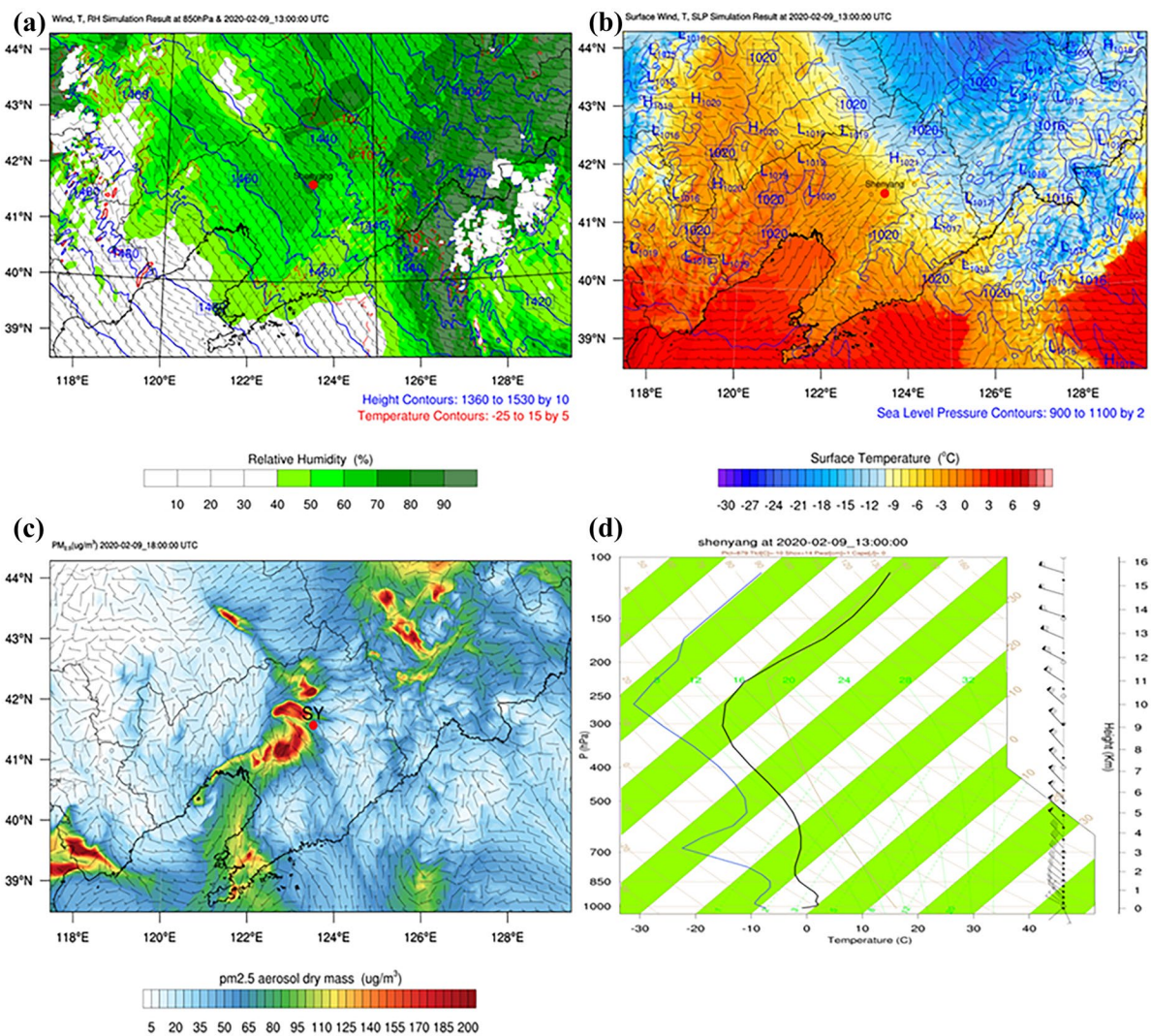
**Fig. 11** Weather map of P1 pollution process

*Analysis of meteorological causes of pollution process*

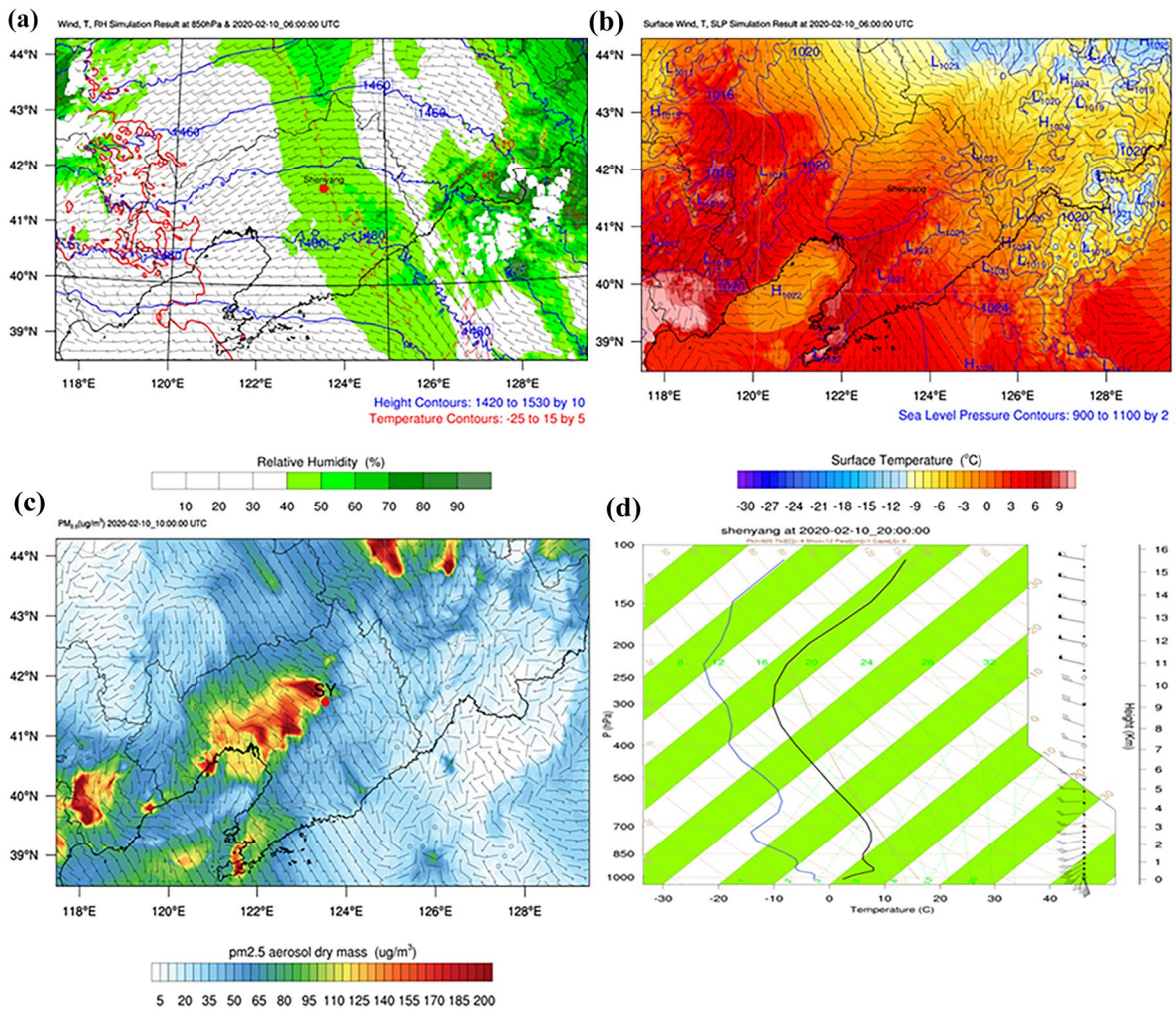
The primary pollutant in the P1 pollution process was PM<sub>2.5</sub>. The simulation results of WRF-Chem were used to reproduce the process of aggregation, dissipation and re-aggregation of PM<sub>2.5</sub>.

Figure 12 shows that on January 9<sup>th</sup>, the wind speed in Shenyang was mostly 2 m/s, the humidity near the ground was relatively high, and the west-southwest wind prevailed. The concentration of particulate matter discharged in the Bohai Sea was

relatively high, and the terrain with high east and low west promotes the accumulation of pollutants carried by trajectories in the northwest and southwest directions on the bottom of the mountain. From the 850 hpa high-altitude map, it could be seen that the high-altitude wind speed was less than 6 m/s. The Shenyang area was located behind the front ridge of the trough, and the ground had a strong compound effect. There was a ground inversion layer near the ground, which reduced the vertical atmospheric mixing rate, and pollutants were prone to accumulation under such weather conditions.



**Fig. 12** The 850 hpa high-altitude weather map (a), surface weather map (b), PM<sub>2.5</sub> concentration map (c) and oblique temperature map (d) on February 9<sup>th</sup>



**Fig. 13** The 850hpa high-altitude weather map (a), surface weather map (b),  $PM_{2.5}$  concentration map (c) and oblique temperature map (d) on February 10<sup>th</sup>

On the 10<sup>th</sup> (Fig. 13), the concentration of pollutants maintained a relatively large value. The surface weather system in Shenyang was dominated by low pressure, the surface temperature was about 4 °C, and the relative humidity was low (40%). In the high-altitude 850hpa weather map, the high-altitude wind speed was small, the thickness of the ground inversion layer increased, and the pollutants concentration continued to rise. Lower wind speed and higher humidity (50%-60%) provided conditions for the formation of secondary particulate matter, which was conducive to the secondary generation of pollutants, resulting in a further decline in air quality.

On the 11<sup>th</sup> (Fig. 14), the weather conditions improved and the temperature increased. The Shenyang area was controlled by the southerly and southwesterly winds, the surface wind speed was small (2 m/s), and the relative humidity decreased by about 30%, reducing the speed of the secondary reaction. In the 850 hpa high-altitude map, the wind speed was southwesterly. The Shenyang area was located in the cold advection control of the high-altitude trough. The atmospheric vertical convection was strong and the disturbance was good, which made the pollutants diluted and diffused and the concentration reduced.

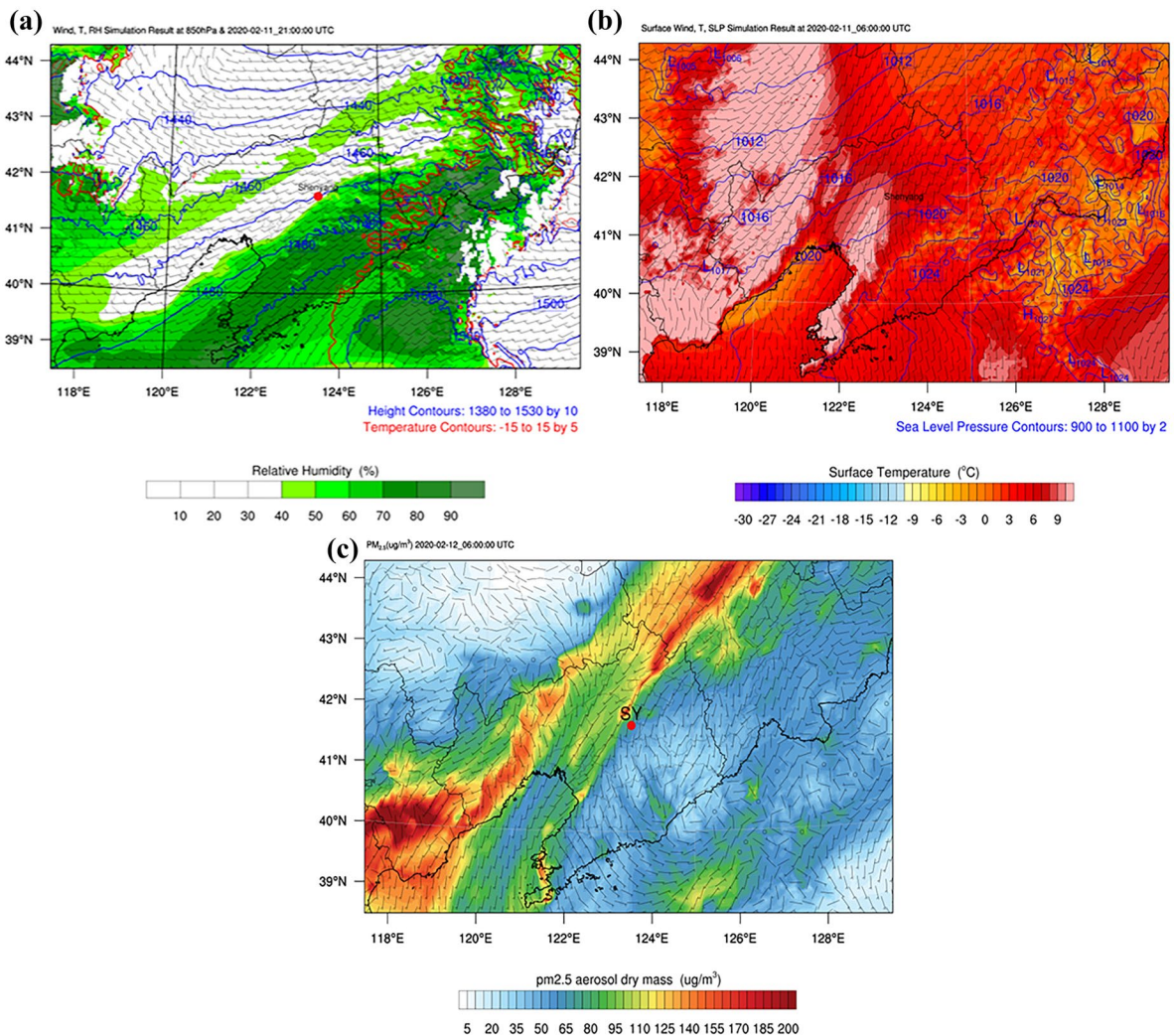


**Fig. 14** The 850 hpa high-altitude weather map (a), surface weather map (b), and PM<sub>2.5</sub> concentration map (c) on February 11<sup>th</sup>

Based on the analysis, the pollution occurred under the weather conditions of high pressure, high humidity, low wind speed and inversion near the ground. There was warm advection at high altitude, and the influence of warm advection would also lead to the decline of air quality. In addition, when the ground was located at the rear of the high-pressure system and the front of the low-pressure system, the southerly wind prevailed on the ground, which could also lead to the aggravation of regional pollution under the influence of the southwest wind.

Table 6 is the comparative analysis of pollutant simulation data and detection data. As data showed, the simulated values were relatively larger than the observed values. MFB and MFE were 21.7% and 65.4%, respectively, which were within the ideal range of simulation (MFB ≤ ±60% and MFE ≤ ±75%). The error obtained in the simulation was caused by a variety of conditions. Herein, the background error in the WRF-Chen model and the spatial uncertainty in the emission inventory added to this error. In general, the simulation results

**Table 6** Statistical analysis of observed and simulated PM<sub>2.5</sub> concentrations

Pollutant	Simulated values	Monitored values	MB	NMB	NME	MFB	MFE
PM <sub>2.5</sub>	69.38 µg/m <sup>3</sup>	64.11 µg/m <sup>3</sup>	5.25 µg/m <sup>3</sup>	8.1%	70.7%	21.7%	65.4%

were able to reproduce the levels of air contaminants during the pollution period.

#### *Influence of external airflow on pollutant concentration*

As shown in Fig. 15a, the typical pollution process P1 clustered the airflow trajectories into 4 categories at a height of 100 m. The most important route corresponded to trajectory 2 (40.91%), which came from Russia to the northeast region of Inner Mongolia Autonomous Region and later to the Liaoning

Province. Trajectory 4 (27.27%) was the second most important route corresponding to the short-range transport in the direction of the Bohai Sea. Finally, trajectory 1 (15.91%) came from Russia and traveled to Liaoning Province via central Heilongjiang and central Jilin. Trajectory 3 (15.91%) also entered from Russian to Liaoning Province via northwestern Heilongjiang and northeastern Inner Mongolia Autonomous Region.

Later, we combined and analyzed the PSCF (Fig. 15b) and CWT (Fig. 5c). According to the method of reference (Lei et al., 2020), WPSCF > 0.5 µg·m<sup>-3</sup>, WCWT > 120 µg·m<sup>-3</sup> were defined as the main contributing

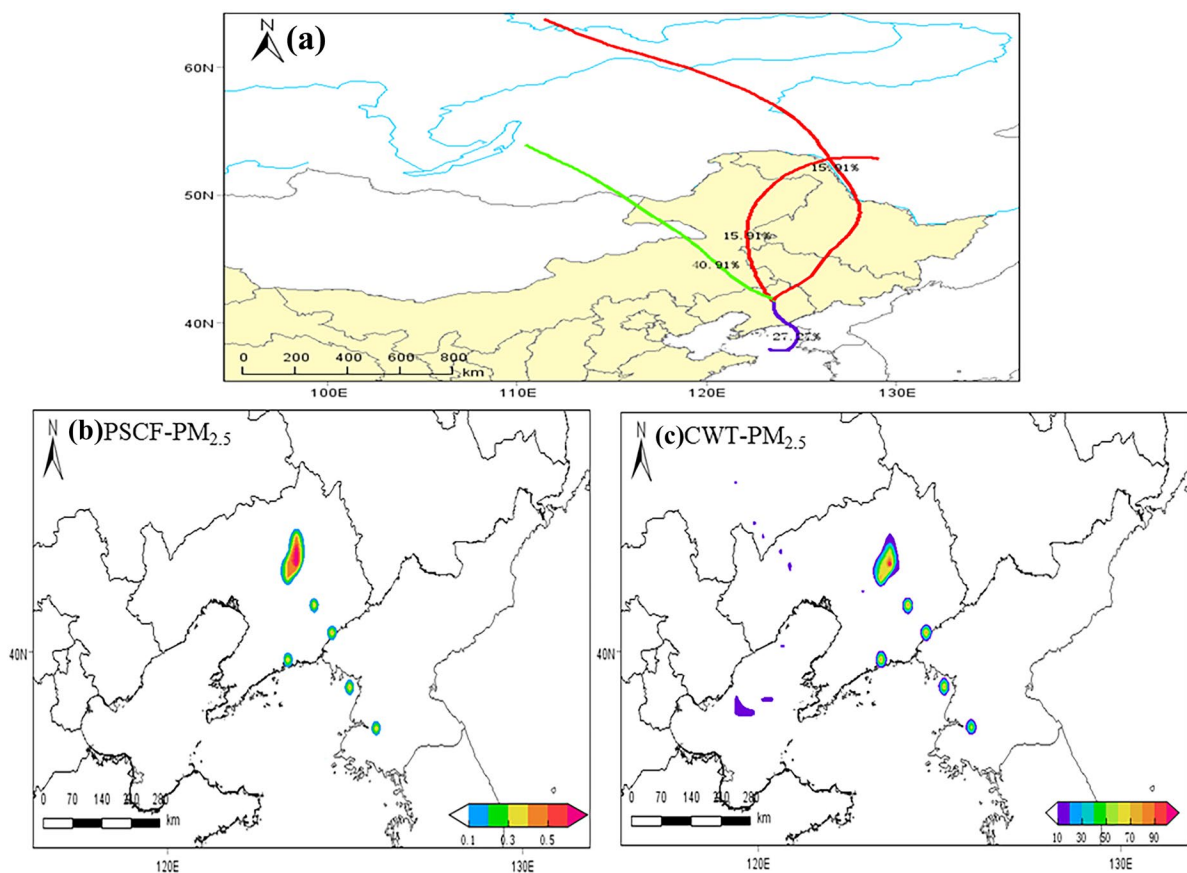


**Fig. 15** (a) Cluster-back trajectories, (b) potential pollution areas and (c) potential pollution concentrations of PM<sub>2.5</sub>

regions. The results showed that WPSCF and WCWT were in good agreement. Data indicated that the P1 pollution process was mainly concentrated in the central Liaoning urban agglomeration around Shenyang and several coastal cities including Dalian, Anshan, Liaoyang, and Dandong, among others. In addition, sporadic contributions came from North Korea. These data showed that, in addition to strengthening local pollution prevention and control while resuming work and production activities, control measures should also be applied to surrounding areas.

## Conclusions

During the blockade period in 2020, the concentration of pollutants significantly increased as compared with the same period in the past 5 years. During the normal period, pollutants concentrations ( $PM_{2.5}$ ,  $PM_{10}$ ,  $NO_2$  and  $O_3$ ) increased by 32.6%, 13.2%, 4.65% and 22.7%, respectively. During the blockade period, concentrations decreased by 35.79%, 35.87%, 32.45% and -4.84% correspondingly. During the resumption period, concentrations increased by 21.8%, 8.7%, 5.7% and -6.3%. During the normal and resumption periods,  $PM_{2.5}$  exceeded the standard value 21 d and 9 d, respectively. With respect to the blockade period, the days exceeding the standard were 8 d.

Pollutants concentrations in various functional areas in Shenyang varied to different degrees. During the normal period, the largest change in pollutants ( $PM_{2.5}$ ,  $PM_{10}$ ,  $NO_2$ ,  $O_3$ ) was the western area, and concentration increased by  $54.24 \mu\text{g}\cdot\text{m}^{-3}$ ,  $49.79 \mu\text{g}\cdot\text{m}^{-3}$ ,  $12.27 \mu\text{g}\cdot\text{m}^{-3}$ , and  $0.12 \mu\text{g}\cdot\text{m}^{-3}$ . During the blockade period, the central area changed most obviously, with the concentrations decreasing by  $23.94 \mu\text{g}\cdot\text{m}^{-3}$ ,  $42.54 \mu\text{g}\cdot\text{m}^{-3}$ ,  $19.65 \mu\text{g}\cdot\text{m}^{-3}$  and  $-5.52 \mu\text{g}\cdot\text{m}^{-3}$ , respectively. During the resumption period, western area changed significantly, with pollutant concentrations increasing by  $23.03 \mu\text{g}\cdot\text{m}^{-3}$ ,  $35.63 \mu\text{g}\cdot\text{m}^{-3}$ ,  $10.59 \mu\text{g}\cdot\text{m}^{-3}$  and -13.22 respectively.

Compared with the same period in the past 5a, the meteorological conditions in 2020 had not changed much. Compared with the same period in previous years, the meteorological conditions in April were relatively unfavorable for photochemical reactions, and  $O_3$  levels decreased.

During the blockade period, when adverse meteorological conditions occurred, heavy pollution weather would still occur, but the emission reduction had a

significant reduction effect on the peak concentration of heavy pollution process. During the blockade, four  $PM_{2.5}$  pollution incidents occurred, one of which showed heavy pollution characteristics. The occurrence of heavy pollution was mainly caused by meteorological conditions. The Shenyang has been exposed to high temperatures (average temperature  $> 10 \text{ }^\circ\text{C}$ ), high humidity (40%–60%), and quiet breeze ( $2 \text{ m}\cdot\text{s}^{-1}$ ) conditions for a long time, and the overall weather did not favor removal and diffusion of pollutants. The backward trajectory showed that the potential source areas of this heavy pollution were concentrated in the urban agglomeration of central Liaoning around Shenyang, and sporadic contributions came from North Korea.

Based on the changes of pollutants, it has brought some inspiration for air pollution control. First, Shenyang is affected by the transmission of pollutants in the southwest and northeast channels, so it is necessary to further strengthen regional control. Second, the current air pollution has obvious complex characteristics, so the next step should be to accurately and quantitatively analyze the sources of pollutants on different spatial scales such as city-region-nation, and scientifically guide the coordinated emission reduction of multiple pollutants.

**Acknowledgements** The research was financially funded by Aeronautical Science Foundation of China (Grant No. 2017ZA54001).

**Author contributions** Yunfeng Ma and Huijie Zhao designed the experiments. Huijie Zhao and Xiangnan Wei performed the experiments, analyzed the results and wrote the paper.

**Data availability statement** The data used to support the findings of this study are available from the corresponding author upon request.

## Declarations

**Conflict of interest** The authors declare that they have no known competing financial interests or personal relationships that could have appeared to influence the work reported in this paper.

## References

- Angelevska, B., Atanasova, V., & Andreevski, I. (2021). Urban air quality guidance based on measures categorization in road transport. *Civil Engineering Journal*, 7(2), 253–267.
- Bao, R., & Zhang, A. (2020). Does lockdown reduce air pollution? Evidence from 44 cities in northern China. *Science of the Total Environment*, 731, 139052.

- Cai, J. Z., Peng, Z., Sun, J. N., Xie, Y. N., & Liu, Q. (2021). Evaluating the impact of the COVID-19 lockdown on the pollutant emissions reduction in Nanjing. *Acta Scientiae Circumstantiae*, 41(08), 2959–2965.
- Chen, J. X., Hu, H., Wang, F. F., Zhang, M., Zhou, T., Yuan, S. C., et al. (2021). Air quality characteristics in Wuhan (China) during the 2020 COVID-19 pandemic. *Environmental Research*, 195.
- Dorling, S. R., Davies, T. D., & Pierce, C. E. (1992). Cluster analysis: A technique for estimating the synoptic meteorological controls on air and precipitation chemistry—method and applications. *Atmospheric Environment Part A General Topics*, 26(14), 2575–2581.
- Draxler, R., & Hess, G. D. (1998). An overview of the HYSPLIT4 modeling system of trajectories, dispersion, and deposition. *Australian Meteorological Magazine*, 47(04), 295–308.
- Eyisi, R., Esonye, C., & Sunday, C. U. (2021). Sustaining COVID-19 pandemic lockdown era air pollution impact through utilization of more renewable energy resources. *International Journal of Environmental Studies*, 7(07), 696–717.
- Feistel, R., & Hellmuth, O. (2021). Relative humidity: A control valve of the steam engine climate. *Journal of Human, Earth and Future*, 2(2).
- Guo, L. P., Qiao, L., Shi, M. H., & Wang, X. G. (2015). Analysis about meteorological conditions of continuous heavy pollution episodes in Langfang of Hebei province. *Journal of Arid Meteorology*, 33(03), 497–504.
- He, W. X., Xu, Y. X., Liao, X., Chen, Q., & Qi, J. (2021). Comparative analysis of the temporal and spatial differences of PM<sub>2.5</sub> and O<sub>3</sub> in Hubei Province at the beginning of 2020 compared with the same period in previous years. *Journal of Baoji University of Arts and Sciences(Natural Science Edition)*, 41(02), 81–92.
- Hu, X., Liu, Q. Z., Fu, Q. Y., Xu, H., Shen, Y., Liu, D. G., et al. (2021). A high-resolution typical pollution source emission inventory and pollution source changes during the COVID-19 lockdown in a megacity, China. *Environmental Science and Pollution Research International*, 28(33), 45344–45352.
- Hua, S. B., Shi, H. D., Wang, K., & Gao, J. J. (2018). Analysis of meteorological conditions for a heavy pollution process in north China during 2016–2017 winter. *Meteorological and Environmental Sciences*, 41(04), 47–53.
- Hsu, Y. K., Holsen, T. M., & Hopke, P. K. (2003). Comparison of hybrid receptor models to locate PCB sources in Chicago. *Atmospheric Environment*, 37(04), 545–562.
- Lei, Y., Zhang, X. L., Kang, P., Wang, H. L., Qing, Q., Ou, Y. H., et al. (2020). Analysis of transport pathways and potential sources of atmospheric particulate matter in Zigong, in south of sichuan province. *Environmental Science*, 41(07), 3021–3030.
- Li, P. R., & Xiang, W. G. (2018). Influence of inversion layer characteristics in Sichuan Basin on air pollution. *Journal of Chengdu University of Information Technology*, 33(02), 220–226.
- Liu, N., Yu, Y., Zhang, Y. L., Wang, Q. H., & Ma, X. Q. (2021). Difference analysis of source and transportation in particulate matter in Xining during 2016–2018. *Environmental Science*, 41(10), 4212–4227.
- Ma, T., Duan, F. K., He, K. B., Qin, Y., Tong, D., Geng, G. N., et al. (2019). Air pollution characteristics and their relationship with emissions and meteorology in the Yangtze River Delta region during 2014–2016. *Journal of Environmental Sciences*, 83(09), 8–20.
- Stohl, A. (1996). Trajectory statistics—A new method to establish source-receptor relationships of air pollutants and its application to the transport of particulate sulfate in Europe. *Atmospheric Environment*, 30(04), 579–587.
- Thangjai, W., Niwitpong, S. A., & Niwitpong, S. (2021). Bayesian confidence intervals for coefficients of variation of PM<sub>10</sub> dispersion. *Emerging Science Journal*, 5(2), 139–154.
- Tian, J., Wang, Q. Y., Zhang, Y., Yan, M. Y., Liu, H. K., Zhang, N. N., et al. (2021). Impacts of primary emissions and secondary aerosol formation on air pollution in an urban area of China during the COVID-19 lockdown. *Environment International*, 150, 11–14.
- Toh, Y. Y., Lim, S. F., & Glasow, R. V. (2013). The influence of meteorological factors and biomass burning on surface ozone concentrations at Tanah Rata, Malaysia. *Atmospheric Environment*, 70, 435–446.
- Wang, L. L., Wang, Y. S., Wang, Y. K., Sun, Y., Ji, D. S., & Ren, Y. F. (2010). Relationship between different synoptic weather patterns and concentrations of atmospheric pollutants in Beijing during summer and autumn. *China Environmental Science*, 30(07), 924–930.
- Wang, Y. T., Zhang, Q., Wen, X. Y., Dou, N. C., Zhao, W. T., Luo, S. Z., et al. (2022). Spatiotemporal distribution and seasonal characteristics of regional transport of PM<sub>2.5</sub> in Yuncheng city. *Environmental Science*, 43(01), 1–16.
- Wu, X., Fang, N. X., Xiong, T., Wang, X., & Ye, C. Q. (2020). Analysis on air pollution characteristics of typical city along the Yangtze River during epidemic control period. *Environmental Science and Technology*, 33(03), 60–64.
- Wu, J., Qi, X. B., Su, J. H., Li, J. F., Sha, C. Y., Xiong, L. J., et al. (2019). Analysis on variation characteristics of PM<sub>2.5</sub> and PM<sub>10</sub> concentration and influence of meteorological factors in Shanghai Chongming Island in 2015. *Meteorological and Environmental Sciences*, 42(03), 1–8.
- Xia, J. Q., Chen, Q., Liu, X., Zhang, R. X., & Li, G. Y. (2021). Transport characteristics and potential source of ozone in Wuhai. *Acta Scientiae Circumstantiae*, 41(08), 3012–3020.
- Xue, W. B., Shi, X. R., Yan, G., Wang, J. N., Xu, Y. L., Tang, Q., et al. (2021). Impacts of meteorology and emission variations on the heavy air pollution episode in North China around the 2020 Spring Festival. *Science China (Earth Sciences)*, 64(02), 329–339.
- Yan, X., Shi, A. J., Cao, J. Y., Li, T. T., Sun, X. S., Zhang, R., et al. (2021). The occurrence of heavy air pollution during the COVID-19 outbreak in Beijing, China: Roles of emission reduction, meteorological conditions, and regional transport. *Meteorological Conditions, and Regional Transport*, 13(21), 12312–12312.
- Yao, R. S., Tu, X. P., Zhang, X. W., Xu, D. F., Yang, D., & Gu, X. L. (2017). Analysis on a rare persistent heavy pollution event in Ningbo. *Acta Meteorologica Sinica*, 75(02), 342–355.
- Yin, X. F., Kang, S. C., R, M., Foy, B. D., Li, P., Yang, J. H., et al. (2021). Influence of transboundary air pollution on air quality in southwestern China. *Geoscience Frontiers*, 12(06), 120–134.

- Yu, G. G., Wang, B. N., Chen, P., Huang, L., & Xie, X. P. (2015). Analysis of characteristics of a long-lasting fog-haze event in Jiangsu 2013. *Meteorological Monthly*, *41*(05), 622–629.
- Zhao, D. L., Tian, P., Zhou, W., Xiao, W., Sheng, J. J., Wang, F., et al. (2021). Evolution and potential source apportionment of atmospheric pollutants of two heavy haze episodes during the COVID-19 lockdown in Beijing. *China Environmental Science*, *42*(11), 1–18.
- Zhou, S., Liu, N., & Liu, C. S. (2017). Identification for potential sources for haze events in Shanghai from 2013 to 2015. *Acta Scientiae Circumstantiae*, *37*(05), 1835–1842.
- Zhou, Y. R., Zhu, K. G., Huang, F., Liu, D., & Liu, W. (2020). Emission reductions and air quality improvements during the COVID-19 pandemic in Hubei province. *Environmental Science & Technology*, *43*(03), 228–236.
- Zhu, Y. Y., Wang, W., Gao, Y. X., Chu, C. J., Xu, R., & Lu, N. (2021). Assessment of emission reduction effect in Beijing, Tianjin and surrounding 26 cities from January to March in 2020 during the epidemic of COVID-19. *China Environmental Science*, *41*(02), 505–516.

**Publisher's Note** Springer Nature remains neutral with regard to jurisdictional claims in published maps and institutional affiliations.

Springer Nature or its licensor holds exclusive rights to this article under a publishing agreement with the author(s) or other rightsholder(s); author self-archiving of the accepted manuscript version of this article is solely governed by the terms of such publishing agreement and applicable law.